energy&fuels

ARTICLE

pubs.acs.org/EF

Anisole and Guaiacol Hydrodeoxygenation over Monolithic Pt−Sn Catalysts

Miguel Ángel González-Borja and Daniel E. Resasco*

Center for Biomass Refining, School of Chemical, Biological, and Materials Engineering, University of Oklahoma, Norman, Oklahoma 73019, United States

ABSTRACT: Direct vapor-phase upgrading of biomass pyrolysis products requires a catalytic reactor able to treat high reactant flow rates without generating a large pressure drop, because conventional pyrolysis reactors operate near atmospheric pressure. Monolithic catalysts exhibit important advantages that make them good candidates for this purpose. In this paper, low-surface-area Inconel monoliths were coated with *in-situ*-grown carbon nanofibers (CNFs), which were subsequently impregnated with catalytic species (Pt, Sn, and bimetallic Pt−Sn). These monoliths were tested for the deoxygenation of guaiacol and anisole (products of lignin pyrolysis), two of the most deactivating compounds present in pyrolysis oil. The main products obtained from these feeds on the monolithic catalysts were phenol and benzene. Coating with CNFs provides increased surface area and anchoring sites for the active species (Pt and Sn), thus increasing the yield of desired products. The bimetallic Pt−Sn catalysts showed higher activity and stability than monometallic Pt and Sn catalysts. These tests indicate that monoliths of Pt−Sn/CNF/Inconel are potentially effective catalysts for the vapor-phase upgrading of lignin fractions present in bio-oil.

1. INTRODUCTION

Among the different processes being investigated for the conversion of biomass to transportation fuels, fast pyrolysis appears as an attractive alternative because it results in a high liquid/feed ratio and does not require extensive capital investments.[1] A recent techno-economical analysis suggests that pyrolysis-derived biofuels are competitive with other alternative fuels, but the technology is relatively immature, which causes uncertainty in some of the estimates.[2] Bio-oil obtained from fast pyrolysis has a high oxygen content, which makes the product unsuitable for transportation fuels. This inadequacy of bio-oil creates the need for novel catalytic processes to upgrade the pyrolysis products with the required stability and fuel properties.[3,4] The compounds present in bio-oil (besides water) can be grouped into five families: hydroxyaldehydes, hydroxyketones, sugars and dehydrosugars, carboxylic acids, and phenolic compounds.[5] Upgrading of this oxygenated mixture has been carried over different types of catalysts. Several studies during the 1990s used zeolites to convert oxygenated model compounds as well as whole bio-oil.[6−8] At the same time, motivated by the obvious advantage of co-processing bio-oil in existing refinery operations, deoxygenation studies of bio-oil model compounds over conventional hydrotreating (HDT) catalysts have been conducted.[9−11] More recently, supported platinum catalysts have been investigated in the upgrading of model bio-oil mixtures.[12] It has been recognized that these catalysts face the challenge of a fast deactivation in the presence of phenolic compounds, which can only be slowed using high hydrogen pressures.

High-pressure post-pyrolysis HDT processes cannot be easily integrated with conventional pyrolysis reactors, because the latter operate at near atmospheric pressure. The only option is therefore to condense the pyrolysis vapors and feed the liquid bio-oil to the HDT units. The great challenge in doing this in large scale is the low chemical and thermal stability of bio-oil. A more desirable option would be to directly feed the vapors coming out of the pyrolysis unit into an upgrading reactor or a cascade of reactors. Therefore, it is highly advantageous to find a catalyst system that can work efficiently in the presence of bio-oil vapors, particularly the severely deactivating phenolic compounds, at atmospheric pressure. An aspect that must be taken into account is the unwanted effect of pressure buildup in the upgrading reactor that might upset the stable operation of the pyrolysis reactor. In this regard, monolithic supports appear as an attractive option because they typically generate minimum pressure drops during operation, even at high flow rates.[13] Thus, we have focused on using monolithic catalyst supports for the proposed upgrading cascade of pyrolysis vapors.

It is well-known that monolithic catalyst supports can be synthesized with low or high surface areas. High-surface-area monoliths are a better choice for catalytic reactions because they allow for higher dispersion of the active material and provide a higher contact area between the catalyst and the gas. However, the synthesis of high-surface-area monoliths is rather expensive, and their mechanical resistance is much lower than that of low-surface-area monoliths.[14] The disadvantages of a low-surface-area monolith can be overcome by coating the substrate with an overlayer of high surface area. For example, washcoating is a widely used method for increasing the surface area of monoliths. Silica and alumina have been commonly used for this purpose by the formation of a thin oxide layer onto the monolith walls, providing a suitable, high-surface-area material for the incorporation of the active phase. Carbon has also been used as a high-surface-area coating for monoliths, and it

Received: May 15, 2011
Revised: July 25, 2011
Published: July 26, 2011

presents good advantages because it is generally inactive for most secondary reactions that may occur on other catalyst supports.[15] For example, the behavior of platinum and palladium catalysts supported on carbon nanofiber (CNF)-coated cordierite monoliths has been recently compared to that of catalysts supported on alumina washcoated monoliths.[16] It was found that the surface area was doubled when CNFs were grown. Also, the adsorption of water on the support (and catalyst deactivation) was reduced because of the higher hydrophobicity of carbon when compared to alumina.

In the area of biomass conversion, monolithic catalyst supports have been used in the production of hydrogen gas from pyrolysis oil,[17−19] and in the cleaning of syngas from biomass gasification.[20,21] However, they have not been used yet in the upgrading of pyrolysis vapors. In this paper, we have investigated Pt−Sn catalysts on CNF-coated monoliths as a novel catalytic upgrading system for the deoxygenation of anisole and guaiacol, chosen as model molecules because they are among the most abundant phenolic compounds derived from lignin pyrolysis.[22]

2. EXPERIMENTAL SECTION

2.1. Materials. The monoliths used in this study were Inconel Metpore exhaust filtration/catalyst support (EFCS), with a relative density of 4.3% and 100 pores per inch. Catalyst metal precursors for nanofiber growth (Cu) and deoxygenation reactions (Pt and Sn) were copper(II) nitrate pentahemihydrate (99%, Riedel-De-Haen), dihydrogen hexachloroplatinate(IV) hexahydrate (99.9%, Alfa Aesar), and tin(II) chloride dihydrate (reagent grade, Alfa Aesar), respectively. Guaiacol (2-methoxyphenol) and anisole (methoxybenzene) were 99% from Sigma Aldrich. Standards for product identification were benzene (99.9%, Sigma Aldrich), toluene (99.7, Alfa Aesar), phenol (99%, Sigma Aldrich), and *o*-cresol (98%, Alfa Aesar). Gases were hydrogen [ultra-high purity (UHP)], nitrogen [high purity (HP)], and ethylene (UHP), all from Airgas.

2.2. Catalyst Synthesis. The Inconel material was shaped into cylinders of diameter equal to the reactor tube diameter and $^1/_2$ in. length. The resulting monoliths were treated with nitric acid solution to remove impurities from the surface and enhance the anchoring of the precursors. After this treatment, the monoliths were washed in deionized (DI) water and dried overnight. These monoliths are referred to as blank/Inconel in the text. Impregnation of single metals (copper for nanofiber growth and platinum and tin for reaction) was performed by sonication for 3 h in a precursor solution that contained 3 wt % of the active metal, followed by room temperature drying for 5 h and overnight drying at 110 °C. This procedure was performed twice. Then, calcination was carried out under flow of air for 2 h at 400 °C for the platinum catalyst and 600 °C for the tin catalyst. Samples impregnated with platinum and tin are referred to as Pt/Inconel and Sn/Inconel, respectively. Platinum and tin co-impregnation was performed following the same procedure used for the individual metals but using a precursor solution containing 1.5 wt % of each metal (3 wt % total metal, Sn/Pt molar ratio of 1.6), and carrying out calcination at 450 °C. This catalyst is referred to as Pt−Sn/Inconel in the text. Catalysts were reduced *in situ* for 2 h under 200 mL/min flow of hydrogen at various temperatures: Pt/Inconel at 330 °C, Sn/Inconel at 600 °C, and Pt−Sn/Inconel at 400 °C. Copper-impregnated Inconel (i.e., Cu/Inconel) was further treated in a continuous flow reactor for growing CNFs on the monolith surface. *In situ* reduction of Cu/Inconel monoliths was carried out under hydrogen flow at 600 °C, and subsequent treatment with ethylene took place at 700 °C for half an hour. Monoliths resulting from this treatment are called CNF/Inconel. The CNF-coated monoliths were co-impregnated with Pt and Sn by the same procedure as described above, calcined at 450 °C, and reduced *in situ* at 400 °C. This catalyst is called Pt−Sn/CNF/Inconel.

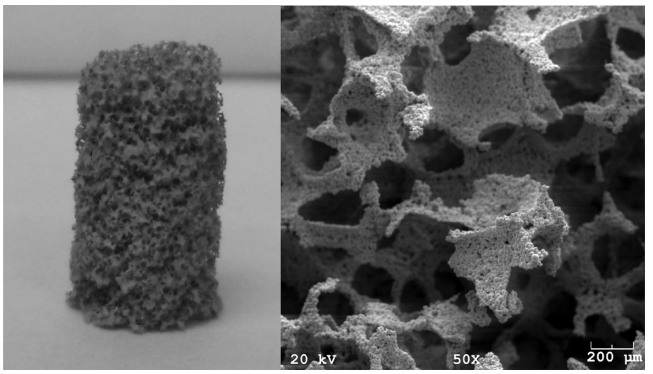

Figure 1. (a) Cylindrical shape of the Inconel monolith and (b) SEM picture showing the monolith structure.

2.3. Catalyst Characterization. The Brunauer−Emmett−Teller (BET) surface area of the catalysts was measured on a Micromeritics ASAP 2000 physisorption apparatus, using N_2 as the probe molecule. The carbon content in the CNF/Inconel sample was determined by two methods, which gave almost identical results. The first method was a direct measurement of the weight difference before and after the CNF growth. The second was thermogravimetric analysis (TGA) on a TGMS Netzsch unit combined with STA 449 Jupiter TG and QMS 403 C Aeolos MS, with a temperature ramp of 10 °C/min, in air. The topography of the catalyst surface was imaged on a Zeiss DSM 960A scanning electron microscope (SEM). The morphology and size of the CNFs and metal particles were investigated on a JEOL 2000-FX transmission electron microscope (TEM).

The metal loading on the monoliths was estimated by assuming that, after the impregnation and calcination steps, the metals were in the form of PtO_2 and SnO, respectively. The weight gained during calcination was used for the estimation of the total metal present in the monolith.

Thermal-programmed reduction (TPR) experiments were performed in a $^1/_4$ in. outer diameter quartz tube. After the catalyst particles were ground and sieved to the size range of 250−425 μm, 30 mg of the monolithic catalyst was treated under 30 mL/min flow of 5% H_2 in Ar, using a temperature ramp of 10 °C/min. Hydrogen consumption was monitored on a thermal conductivity detector (TCD), using Ar as the reference gas.

2.4. Catalytic Reaction. Deoxygenation of anisole and guaiacol was carried out at atmospheric pressure and 400 °C in a quartz tube of $^3/_8$ in. outer diameter and 12.5 in. length. In a typical experiment, the liquid reactant (guaiacol or anisole) was injected from a syringe pump (0.1 mL/h) to a heated stainless-steel tube, where it was mixed with a gas mixture (50 mL/min) stream of N_2 (83%) and H_2 (17%) and vaporized before entering the reactor. The hydrogen/phenolic compound molar feed ratio was 30:1. Products were analyzed online using a Varian 3800 gas chromatograph (GC) equipped with a Rxi-5Sil mass spectrometry (MS) column and flame ionization detector (FID). Liquid products were condensed in an acetone/ice trap. Identification of products in the collected liquid was performed with a GCMS-QP2010S system equipped with a HP-5 column and confirmed by injection of standards to the GC−FID.

3. RESULTS AND DISCUSSION

3.1. Catalyst Characterization. Figure 1a shows a photograph of the Inconel monolith used as a catalyst support, while the low-magnification SEM picture in Figure 1b illustrates the geometry of the monolith openings. The random nature of the

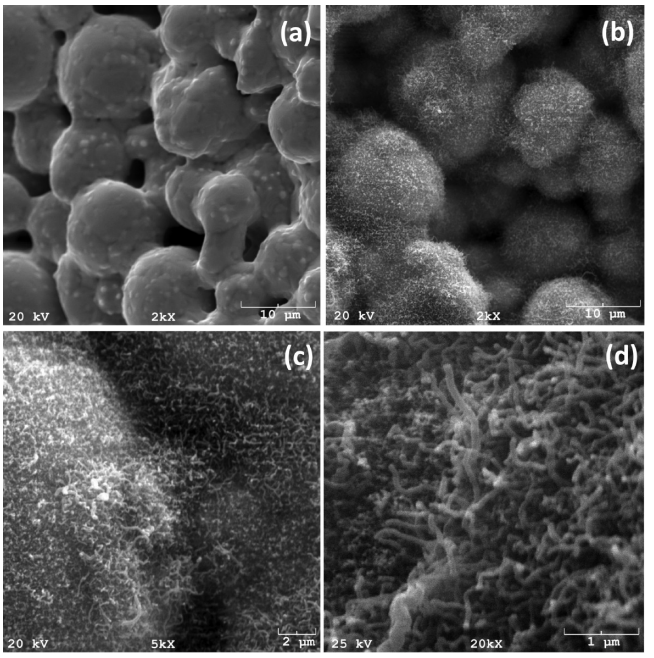

Figure 2. SEM pictures of monolithic catalysts: (a) blank/Inconel, (b and c) CNF/Inconel, and (d) high magnification image to show the CNF.

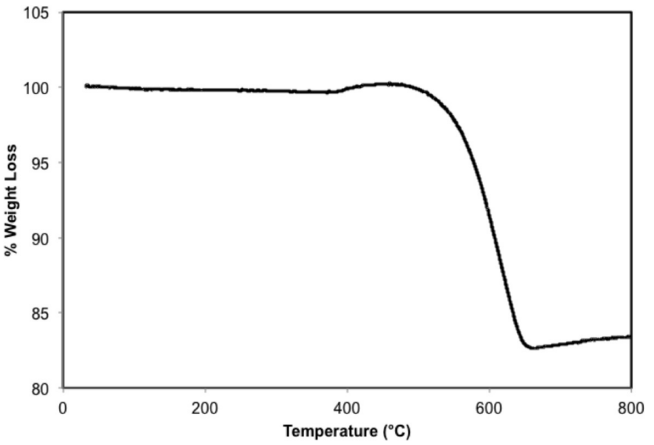

Figure 3. CNFs burn off profile in the CNF/Inconel catalyst.

channels is favorable for the reaction because it provides improved contact between the gas and the catalyst surface. A closer look at the blank/Inconel and CNF/Inconel in Figure 2 reveals the surface of the metal monolith before and after treatment with ethylene at high temperatures. The higher magnification images in panels c and d of Figure 2 show more details of the morphology of the surface covered by CNFs. In addition to the images, energy-dispersive X-ray spectroscopy (EDS) analysis, performed on the same SEM, gave evidence for the high carbon coverage of the surface.

Because the main purpose for growing CNFs on the monolith was to increase the support surface area, the BET surface area of the CNF-coated monolith was compared to that of the bare monolith. The results were 14 ± 1 m^2/g of monolith for CNF/Inconel and less than 1 m^2/g of monolith for the blank/Inconel sample.

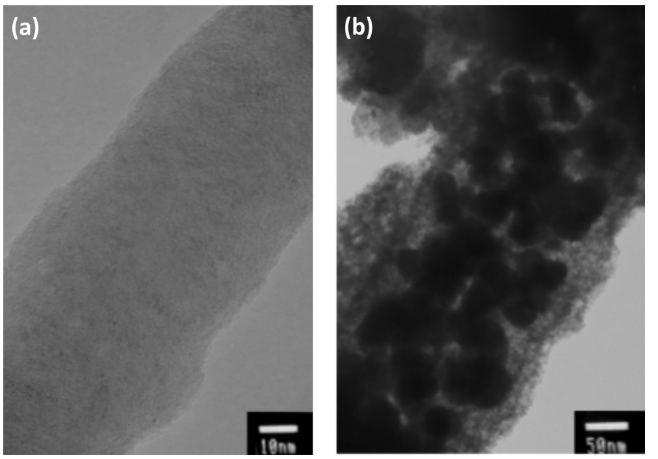

Figure 4. TEM pictures of CNFs (a) before impregnation with Pt−Sn and (b) after impregnation with Pt−Sn and calcination.

The carbon content of CNF/Inconel measured by two different methods gave practically the same result. The weight difference after CNF growth was 17.0 wt %, while TGA by oxidation of the CNF between 30 and 800 °C indicated a weight loss of 16.7 wt % (see Figure 3). On the basis of this carbon content and surface area measurements, the support surface area was estimated to be 82 ± 1 m^2/g of CNF. This value is in good agreement with previous reports for the specific surface area of CNFs.[23] Figure 3 shows the weight loss (carbon burn off) of CNF/Inconel as a function of the temperature. Combustion of the CNFs starts taking place at above 500 °C (see Figure 3). Therefore, it is expected that, after calcination in air at 450 °C, consumption of the support because of combustion of the fibers should not be significant.

Sonication experiments of a CNF/Inconel sample were performed to evaluate the mechanical integrity of the carbon coating during the incorporation of the metal and handling of the monoliths. In this test, an as-prepared monolithic catalyst was dipped in water/acetone solution and placed in a sonication bath under the same conditions used for the impregnation of the active phase. A total weight loss of less than 1 wt % was observed, which indicates that the carbonaceous support is strongly bound to the Inconel surface.

The TEM images in Figure 4 illustrate the morphology of the CNFs present on the monoliths (50−200 nm in diameter), both before and after the Pt−Sn impregnation/calcination steps, giving additional evidence to the mechanical integrity preserved during the process. Figure 4b shows the presence of metal particles anchored on the CNF surface with sizes around 50 nm and above.

TPR experiments were conducted to investigate the formation of Pt−Sn alloys. Figure 5 shows the TPR profiles of the supports before metal impregnation (i.e., blank/Inconel and CNF/Inconel), monometallic catalysts (Pt/Inconel and Sn/Inconel), and bimetallic catalysts (Pt−Sn/Inconel and Pt−Sn/CNF/Inconel). As expected, blank/Inconel shows very low hydrogen consumption; two small peaks are observed, one at 400 °C and one at 510 °C. This small hydrogen consumption can be ascribed to the reduction of some of the constituents of the Inconel alloy. As described below, these reduced metal species do not generate any significant catalytic activity for the reactions of interest. CNF/Inconel does not show any consumption of hydrogen, which

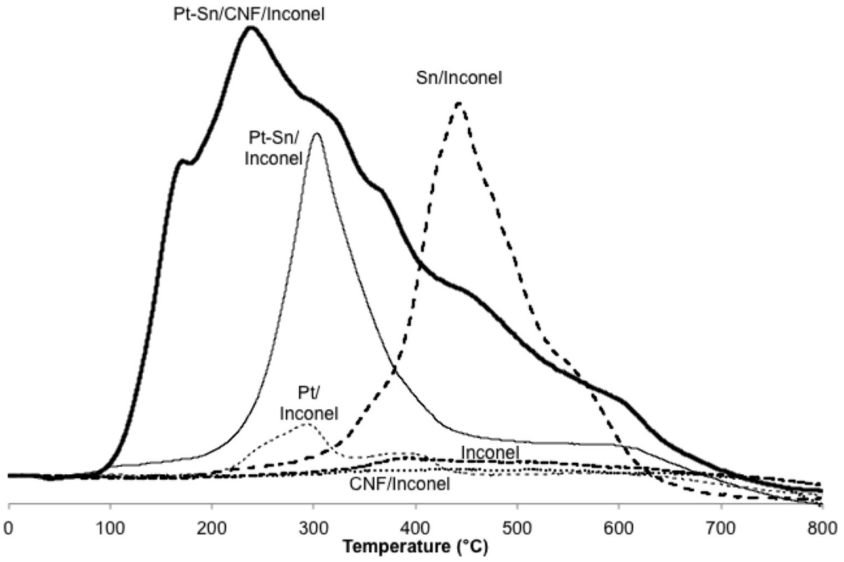

Figure 5. TPR profiles for catalyst supports, monometallic catalysts, and bimetallic catalysts.

Table 1. Catalyst Metal Loading and Initial Activity

catalyst	estimated metal loading (wt %)	initial conversion [mol h^{-1} (g of metal)$^{-1}$]	initial benzene yield [mol h^{-1} (g of metal)$^{-1}$]
Sn/Inconel	8.01	0.008	0
Pt/Inconel	3.38	0.024	0.001
Pt−Sn/Inconel	7.25	0.034	0.012
Pt−Sn/CNF/Inconel	16.21		0.020

suggests that the Inconel surface and the copper particles used for the CNF growth are fully covered by the fibers, so that the metal sites are not able to react with hydrogen.

For the Pt/Inconel catalyst, two hydrogen consumption peaks are observed, one at 300 °C and another at 400 °C. The latter can be attributed to the partial reduction of the Inconel support, because it appears at the same temperature as one of the peaks identified in the blank/Inconel sample. Therefore, the peak at 300 °C is assigned to the reduction of Pt. Sn/Inconel shows a main reduction peak at 450 °C accompanied by a smaller peak at around 550 °C. Previous TPR studies[24] of Pt−Sn/Al_2O_3 catalysts have shown the existence of reduction peaks at 250 °C for Pt and 400 °C for Sn (including a shoulder near 500 °C). Taking into account the difference in the type of support (Inconel versus Al_2O_3) and the differences in the metal particle size (greater in our case), our results are in good agreement with previous experiments. The reduction profile for Pt−Sn/Inconel exhibits a single peak centered around 300 °C, and shows no hydrogen consumption in the region where unalloyed Sn is not present, whereas Pt−Sn/CNF/Inconel presents multiple reduction peaks ranging from 160 to 600 °C. Excess Pt is present and a fraction of it may not be forming the Pt−Sn complex in solution. Therefore, unalloyed Pt is expected on the surface of Pt−Sn/Inconel. The appearance of multiple peaks in the reduction of Pt−Sn/CNF/Inconel can be attributed to a wide distribution in the metal particle size, as observed with TEM, causing the reduction of the alloy to occur in several steps. Furthermore, carboxyl and carbonyl groups are present on the support surface as a result of the oxidation of the fibers.[25] These oxidized species act as anchoring sites for the metal species,[26] which may provide a different degree of interaction between the metal precursors and the supports. This interaction may hinder the mobility of the impregnated species on the surface and may result in the formation of non-uniform alloy particles, which would result in many reduction peaks in the TPR profile.

To investigate whether during the catalyst impregnation there is selective adsorption of the metal precursors, the solutions were analyzed by ultraviolet−visible (UV−vis) spectroscopy before and after being in contact with the substrate. No significant changes in the concentration were observed in the solutions after two consecutive impregnation steps, while progressive weight gains were observed in the monoliths. That is, the metal incorporation onto the monolith is a direct impregnation rather than adsorption of precursor molecules from solution. The precursor solution wets the high-area surface of the monolith, and as the solvent evaporates, the active species remain occluded on the surface. Metal loadings for both mono- and bimetallic catalysts are reported in Table 1.

3.2. Guaiacol Deoxygenation on Mono- and Bimetallic Catalysts. Table 1 reports the initial activity and benzene yield (5 min on stream) on a metal weight basis for mono- and bimetallic catalysts. The blank/Inconel monolith without any metal impregnation showed low conversion, i.e., less than about 3% (not shown). Traces of phenol were observed as the main product. When either Pt or Sn was incorporated onto the monoliths, the guaiacol conversion increased.

The variation of guaiacol conversion, at 1 atm and 400 °C, as a function of time on stream (TOS) is compared in Figure 6 for mono- and bimetallic catalysts. The Pt/Inconel monolith had higher initial activity (see Table 1), but it rapidly deactivated; after 3 h on stream, its activity was that of the blank/Inconel monolith. While the initial activity of Sn/Inconel was lower than that of Pt/Inconel, the deactivation was less severe and, after 3 h on stream, was able to maintain about half of its initial activity. When Pt and Sn were co-impregnated on the bare Inconel surface, the initial activity showed a significant improvement with

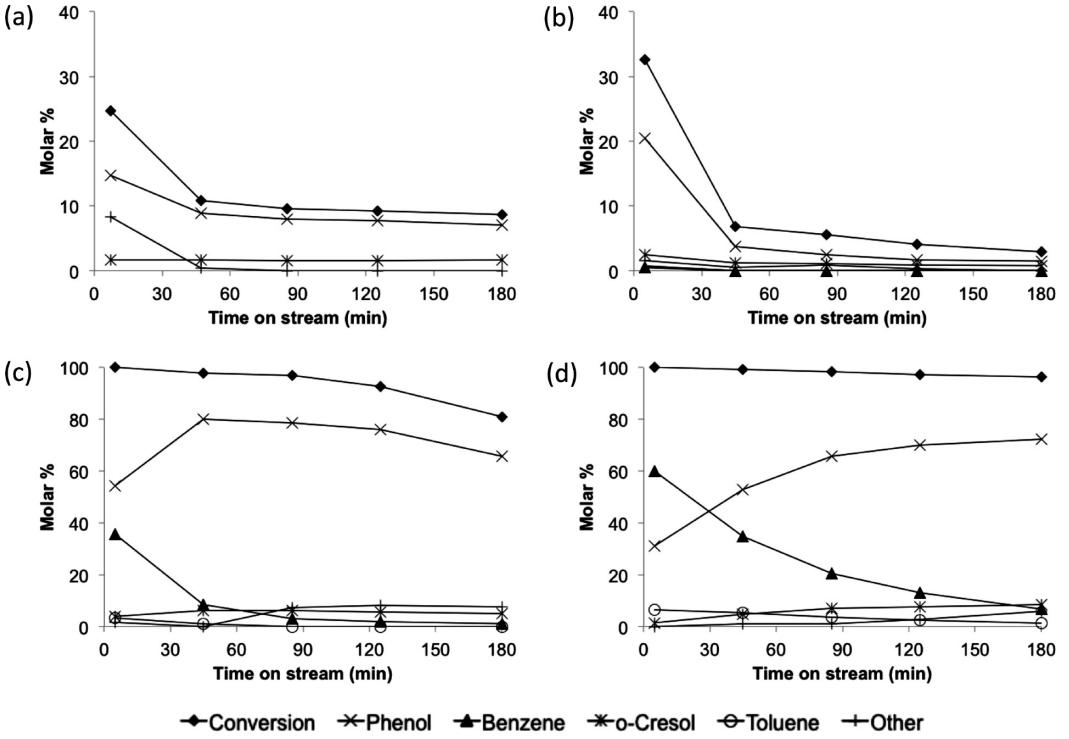

Figure 6. Guaiacol conversion and product yields over different catalysts as a function of TOS at 1 atm and 400 °C: (a) Sn/Inconel, (b) Pt/Inconel, (c) Pt−Sn/Inconel, and (d) Pt−Sn/CNF/Inconel. W/F is 3.2 g of catalyst (g of reactant)$^{-1}$ h^{-1}.

respect to the Pt/Inconel monolith (see Table 1). Both Pt−Sn/Inconel and Pt−Sn/CNF/Inconel catalysts reached 100% conversion of guaiacol initially.

The product distribution as a function of TOS is also shown in Figure 6. Phenol is the main product for both Sn/Inconel and Pt/Inconel, accompanied by a smaller amount of *o*-cresol. Several studies have reported phenol to be an important compound in guaiacol deoxygenation, as either a main product or an intermediate to further deoxygenation.[27−31] Other products included di- and trimethyl phenols, while only traces of anisole and catechol were observed. In the reaction on Pt/Inconel, a small amount of benzene was observed at short TOS but, after the catalyst deactivated, benzene was not longer produced.

While complete hydrodeoxygenation of guaiacol on conventional hydrotreating metal catalysts only occurs at high hydrogen pressures,[30,32] the bimetallic Pt−Sn monolithic catalysts described here are able to fully deoxygenate guaiacol at atmospheric pressure. In contrast, on the monometallic monoliths (either Pt or Sn), full deoxygenation was either not achieved or it occurred to a very small extent. The fast deactivation that occurs in the absence of the alloy is responsible for the rapid loss of deoxygenation activity.

Not only the metallic composition but also the nature of the substrate seems to have an important impact on the performance of the monolith. For instance, Figure 6c summarizes the product yields over the Pt−Sn/Inconel monolith as a function of TOS. Phenol, *o*-cresol, toluene, and benzene were observed in the products. Initially, the C6 products (phenol and benzene) were obtained in about the same proportion, while the C7 products were present in smaller amounts. At longer TOS, the catalyst deactivates and the product distribution showed a lower concentration of fully deoxygenated products,

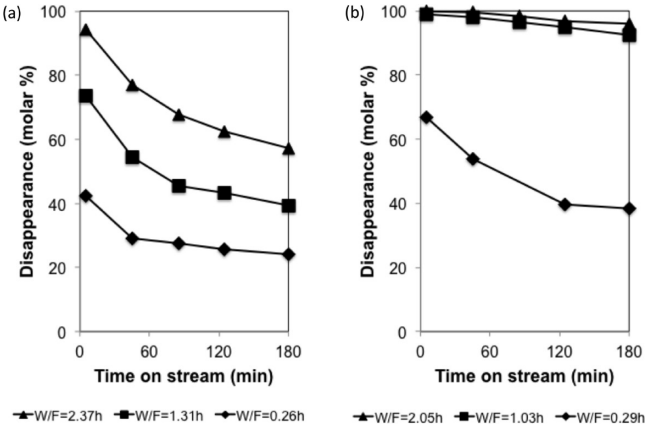

Figure 7. Pt−Sn/CNF/Inconel catalyst deactivation for two different reactants at 1 atm and 400 °C: (a) anisole and (b) guaiacol. W/F is g of catalyst (g of reactant)$^{-1}$ h^{-1}.

which dropped to almost zero after 3 h on stream, with the concomitant increase in the yield of mono-oxygenated phenol and cresols.

For comparison, Figure 6d shows that the Pt−Sn bimetallic catalysts supported on the CNF-coated monolith displayed a much improved performance (see the initial benzene yield in Table 1). In this case, at the beginning of the run, the yield of benzene was higher than that of phenol and, while the product distribution still changed as a function of TOS, the yield of fully deoxygenated products was still significant after 2 h on stream. It is evident that the complete deoxygenation of guaiacol is a sequential reaction that has the mono-oxygenated compounds as intermediate products. Therefore, while the feed conversion is

dx.doi.org/10.1021/ef200728r |*Energy Fuels* 2011, 25, 4155–4162

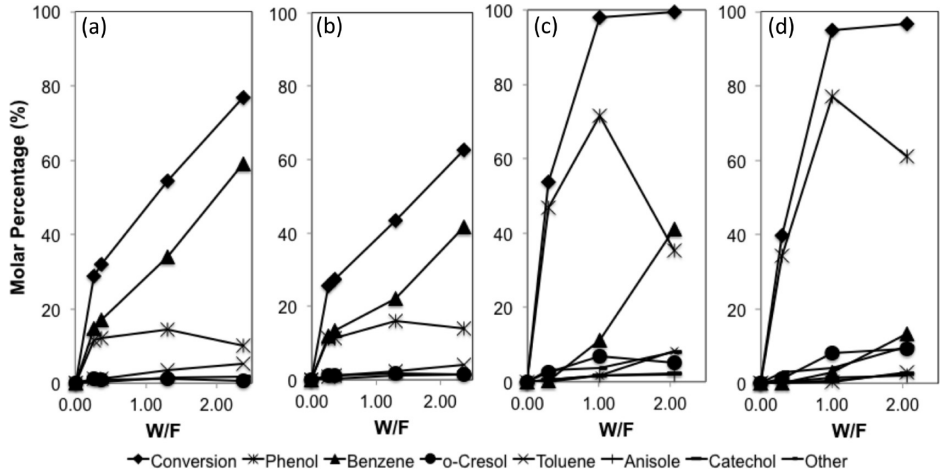

Figure 8. Product yields over the Pt−Sn/CNF/Inconel catalyst for different reactants: (a) anisole with TOS of 45 min, (b) anisole with TOS of 125 min, (c) guaiacol with TOS of 45 min, and (d) guaiacol with TOS of 125 min. W/F is g of catalyst (g of reactant)$^{-1}$ h^{-1}. T = 400 °C, and P = 1 atm.

close to 100% in all cases, when the catalyst is less active or deactivates faster, the selectivity to fully deoxygenated products decreases.

In this comparison, a relatively low initial activity is observed with the Sn/Inconel and Pt/Inconel monoliths (Figure 6). When platinum and tin were co-impregnated on the monolith surface, the initial activity of the catalyst significantly increased (100% conversion), as observed in Table 1. This difference is a good indication of the superior properties of the bimetallic catalyst, most likely because of the formation of the Pt−Sn alloys identified by TPR. In fact, Pt−Sn alloys are widely recognized as stable and selective catalysts for a number of reactions,[33] including some related to biofuel upgrading.[34]

When CNFs were grown on the Inconel monolith surface, the performance of the resulting Pt−Sn catalyst was even better. While the initial guaiacol conversion was already 100% on the Pt−Sn/Inconel monolith, the CNF/Inconel monolith not only had a 100% conversion but also a higher benzene yield (see Table 1). The enhanced surface area generated by the CNFs can clearly improve the uptake of metal (as shown in Table 1) and possibly increases the metal surface that is available for the reaction to take place. A similar positive effect has been reported with other CNF catalysts.[16]

3.3. Comparison of Guaiacol and Anisole Deoxygenation on the Bimetallic Catalyst. On the basis of the superior performance displayed by the Pt−Sn/CNF/Inconel monolith, the rest of the studies were conducted on this catalytic material. For instance, a comparison was made on this monolith for the deoxygenation reactions of guaiacol and anisole. The overall feed conversion at different contact times and space times (W/F) is compared in Figure 7. It is obvious that guaiacol is much more reactive than anisole; only at the lowest W/F investigated, the reactant disappearance was less than 100%. However, despite a higher reactivity, guaiacol shows a higher rate of catalyst deactivation that is only apparent in the distribution of products because the total conversion is 100% and obviously deactivation cannot be measured.

As illustrated in panels a−d of Figure 8, the difference in reactivity and degree of deactivation causes some important differences in the distribution of products obtained from anisole and guaiacol as a function of W/F at different TOS. For instance, the conversion of anisole yields benzene as the main end product, with phenol as the major intermediate, while *o*-cresol and toluene appear as minor products. Other products, such as methylanisole, were observed only in traces. A comparison between panels a and b of Figure 8 shows that, with anisole feed, benzene remains as the main product, even after 125 min on stream. That is, while some degree of catalyst deactivation is apparent, full deoxygenation is still possible. In the case of the guaiacol feed, after the same TOS as those used for anisole (45 and 125 min), phenol dominates over benzene at almost every W/F investigated, with the latter becoming more important only at the highest W/F. As in the case of anisole, toluene and *o*-cresol are observed only as minor products. Catechol (obviously not observed from anisole) appears as a minor product from guaiacol. Dimethoxybenzene and polymethyl phenols are also observed in low concentrations (panels c and d of Figure 8). Analysis of noncondensable gases from the reaction of guaiacol and anisole showed the presence of methane, which can be expected from the hydrogenolysis of the methoxy group.

A series of pulse experiments with anisole and guaiacol were performed to identify the different interactions of these molecules with the catalyst surface. In each experiment, 61 mg of the catalyst was heated up to 400 °C and, subsequently, two 9.5 × 10^{-8} mol pulses were injected 5 min apart onto the catalyst bed in a 100 mL/min He carrier flow. A significant fraction of the injected feed was captured by the catalyst. With anisole, 74% of the first pulse and 39% of the second pulse were retained. With guaiacol, 90% of the pulse was retained in both pulses. It is clear that both molecules adsorb strongly on the catalyst, but some differences are apparent. Anisole preferentially adsorbs on the strongest sites, and a significant fraction of them are occupied during the first pulse, causing the observed decrease in anisole retention during the second pulse. In contrast, guaiacol seems to adsorb on a broader range of sites (strong and weak). As a consequence, the amount of guaiacol retained by the catalyst is the same during both pulses (and higher than anisole). The observed stronger adsorption of guaiacol compared to anisole agrees with the higher reactivity observed with this feed, but at the same time, also agrees with the more severe deactivation observed with guaiacol compared to anisole.

The different extent of catalyst deactivation caused by the two different feeds can be best evaluated by analyzing the yield of fully deoxygenated products as a function of TOS. For instance,

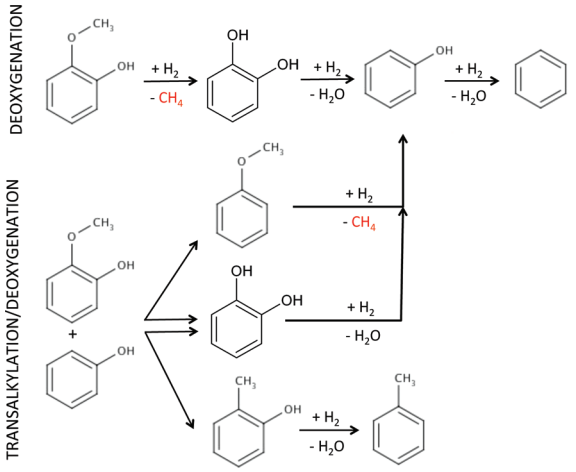

Figure 9. Reaction steps for guaiacol deoxygenation on the Pt−Sn/CNF/Inconel catalyst.

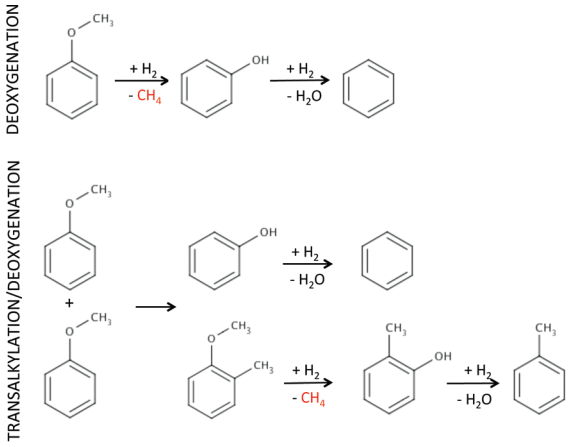

Figure 10. Reaction steps for anisole deoxygenation on the Pt−Sn/CNF/Inconel catalyst.

Figure 8 shows that, while benzene remains as the most abundant product from the deoxygenation of anisole for at least the first 2 h, it is only most abundant at the very beginning of the run when using guaiacol as a feed. Clearly, the catalyst is more severely deactivated by guaiacol (or its products) than by anisole (or its products). As mentioned above, guaiacol first produces catechol, followed by deoxygenation to phenol and finally benzene. In turn, anisole first produces phenol, which is then deoxygenated to benzene. Other studies currently taking place in our group showed that catechol adsorbs more strongly than phenol on different catalyst surfaces (metals, acids, and oxides); in parallel, the pulse experiments reported here give evidence for the stronger adsorption of guaiacol compared to anisole. That is, the double-functionalized guaiacol and catechol are more likely to remain on the surface, blocking deoxygenation sites of phenol to benzene than the single functionalized ones, anisole and phenol.

The observed variation of product distribution with W/F and TOS in the conversion of guaiacol and anisole is consistent with the simplified reaction pathways previously proposed by us and others[22−29,32,35,36] (see Figures 9 and 10). The deoxygenation path starts with decomposition of the methoxy group. Both metals and acids can catalyze this reaction. In this case, the metal function dominates, and it is expected that this step occurs via hydrogenolysis of the C−O bond, producing methane as the gaseous product, experimentally observed. At the same time, the decomposition of the methoxy group results in catechol or phenol from guaiacol and anisole, respectively. Thermodynamically, this C−O bond is weaker than the C−O bond connecting methoxyl to the aromatic ring and weaker than the C−O bond of the hydroxyl group.[32] Therefore, producing catechol from guaiacol is more favorable than directly producing anisole or phenol. However, only traces of catechol are observed in the product from guaiacol, which suggests that catechol is rapidly converted to phenol, perhaps before it desorbs from the metal surface. In contrast, on acid catalysts,[35] catechol is a major product because it is much less reactive. We have also recently shown that another route for the conversion of phenolics is transalkylation, in which the methyl group from methoxyl is transferred to another aromatic molecule. Through this transalkylation path, catalyzed by acid sites,[31,32,35] two anisole molecules can form phenol and methylanisole and later cresol. The subsequent metal-catalyzed deoxygenation of these compounds will produce benzene, phenol, and toluene, respectively. In a similar way, guaiacol can undergo transalkylation and deoxygenation to produce benzene and toluene.

The very low yields of toluene and mono-oxygenated alkylated phenolics (cresol, methylanisole, etc.), together with the significant amounts of methane observed in this case, are consistent with the low acidity of the substrate used in these monoliths, Inconel alloy (support) and CNFs (coating), and show that the main catalytic function for the methoxyl decomposition on these monoliths is metallic. However, the mechanism for hydrodeoxygenation of catechol and phenol may involve some weak acid sites. It is possible that, in addition to a direct C−O cleavage, deoxygenation occurs via (partial) hydrogenation of the aromatic ring followed by dehydration.[32,37] At the low pressures and rather high temperatures used in this study, no ring hydrogenated products are expected to be present in the vapor phase, however, considering the presence of a partially hydrogenated surface intermediate is not unjustified.[38]

4. CONCLUSION

Mono- and bimetallic (Pt−Sn alloy) monoliths were synthetized and tested for the deoxygenation of guaiacol and anisole. Both Pt−Sn/Inconel and Pt−Sn/CNF/Inconel are able to fully deoxygenate guaiacol and anisole. Coating with CNFs increased the surface area of the monoliths more than 10 times, allowing for a higher metal uptake during the active-phase incorporation, when compared to monoliths without coating. Deactivation of the catalyst still needs to be improved; however, the Pt−Sn/CNF/Inconel monolith is a promising catalyst for the upgrading of pyrolysis bio-oil.

AUTHOR INFORMATION

Corresponding Author

*Telephone: (405) 325-4370. E-mail: resasco@ou.edu.

ACKNOWLEDGMENT

This work has been supported, in part, by the National Science Foundation (NSF EPSCoR Award EPS0814361 and MRI NSF Grant 0923247) and the Department of Energy (DE-FG36GO88064).

Miguel Ángel González-Borja thanks Dr. M. P. Ruiz, Dr. R. Jentoft, J. Brown, A. T. To, and M. Wulfers for their expert assistance in the characterization of the monoliths.

REFERENCES

(1) Demirbas, A. Biomass resource facilities and biomass conversion processing for fuel and chemicals. *Energy Convers. Manage.* **2001**, *42*, 1357–1378.

(2) Wright, M. M.; Satrio, J. A.; Brown, R. C.; Daugaard, D. E.; Hsu, D. D. Techno-economic analysis of biomass fast pyrolysis to transportation fuels. *Technical Report NREL/TP-6A20-46586*; National Renewable Energy Laboratory (NREL): Golden, CO, Nov 2010.

(3) Elliott, D. C.; Hart, T. R. Catalytic hydroprocessing of chemical models for bio-oil. *Energy Fuels* **2009**, *23*, 631–637.

(4) Resasco, D. E.; Crossley, S. Molecular engineering approach in the selection of catalytic strategies for upgrading of biofuels. *AIChE J.* **2009**, *55*, 1082–1089.

(5) Mohan, D.; Pittman, C. U., Jr.; Steele, P. H. Pyrolysis of wood/biomass for bio-oil: A critical review. *Energy Fuels* **2006**, *20*, 848–889.

(6) Sharma, R. K.; Bakhshi, N. N. Catalytic upgrading of biomass-derived oils to transportation fuels and chemicals. *Can. J. Chem. Eng.* **1991**, *69*, 1071–1081.

(7) Adjaye, J. D.; Bakhshi, N. N. Catalytic conversion of a biomass-derived oil to fuels and chemicals I: Model compound studies and reaction pathways. *Biomass Bioenergy* **1995**, *8*, 131–149.

(8) Adjaye, J. D.; Bakhshi, N. N. Catalytic conversion of a biomass-derived oil to fuels and chemicals II: Chemical kinetics, parameter estimation and model predictions. *Biomass Bioenergy* **1995**, *8*, 265–277.

(9) Donnis, B.; Egeberg, R. G.; Blom, P.; Knudsen, K. G. Hydroprocessing of bio-oils and oxygenates to hydrocarbons. Understanding the reaction routes. *Top. Catal.* **2009**, *52*, 229–240.

(10) Huber, G. W.; Iborra, S.; Corma, A. Synthesis of transportation fuels from biomass: Chemistry, catalysts, and engineering. *Chem. Rev.* **2006**, *106*, 4044–4098.

(11) Furimsky, E. Catalytic hydrodeoxygenation. *Appl. Catal., A* **2000**, *199*, 147–190.

(12) Fisk, C. A.; Morgan, T.; Ji, Y.; Crocker, M.; Crofcheck, C.; Lewis, S. A. Bio-oil upgrading over platinum catalysts using *in situ* generated hydrogen. *Appl. Catal., A* **2009**, *358*, 150–156.

(13) Pangarkar, K.; Schildhauer, T. J.; van Ommen, J. R.; Nijenhuis, J.; Kapteijn, F.; Moulijn, J. A. Structured packings for multiphase catalytic reactors. *Ind. Eng. Chem. Res.* **2008**, *47*, 3720–3751.

(14) Cybulski, A.; Moulijn, J. A. Monoliths in heterogeneous catalysis. *Catal. Rev.—Sci. Eng.* **1994**, *36*, 179–270.

(15) Nijhuis, T. A.; Beers, A. E. W.; Vergunst, T.; Hoek, I.; Kapeijn, F.; Moulijn, J. A. Preparation of monolithic catalysts. *Catal. Rev.—Sci. Eng.* **2001**, *43*, 345–380.

(16) Morales-Torres, S.; Perez-Cadenas, A. F.; Kapteijn, F.; Carrasco-Marin, F.; Maldonado-Hodar, F. J.; Moulijn, J. A. Palladium and platinum catalysts supported on carbon nanofiber coated monoliths for low-temperature combustion of BTX. *Appl. Catal., B* **2009**, *89*, 411–419.

(17) Basagiannis, A. C.; Verykios, X. E. Steam reforming of the aqueous fraction of bio-oil over structured $Ru/MgO/Al_2O_3$ catalysts. *Catal. Today* **2007**, *127*, 256–264.

(18) Iojoiu, E. E.; Domine, M. E.; Davidian, T.; Guilhaume, N.; Mirodatos, C. Hydrogen production by sequential cracking of biomass-derived pyrolysis oil over noble metal catalysts supported on ceria-zirconia. *Appl. Catal., A* **2007**, *323*, 147–161.

(19) Domine, M. E.; Iojoiu, E. E.; Davidian, T.; Guilhaume, N.; Mirodatos, C. Hydrogen production from biomass-derived oil over monolithic Pt- and Rh-based catalysts using steam reforming and sequential cracking processes. *Catal. Today* **2008**, *133−135*, 565–573.

(20) Torres, W.; Pansare, S. S.; Goodwin, J. G., Jr. Hot gas removal of tars, ammonia, and hydrogen sulfide from biomass gasification gas. *Catal. Rev.—Sci. Eng.* **2007**, *49*, 407–456.

(21) Pinto, F.; André, R. N.; Franco, C.; Lopes, H.; Gulyurtlu, I.; Cabrita, I. Co-gasification of coal and wastes in a pilot-scale installation 1: Effect of catalysts in syngas treatment to achieve tar abatement. *Fuel* **2009**, *88*, 2392–2402.

(22) Mullen, C. A.; Boateng, A. A. Chemical composition of bio-oils produced by fast pyrolysis of two energy crops. *Energy Fuels* **2008**, *22*, 2104–2109.

(23) De Jong, K. P.; Geus, J. W. Carbon nanofibers: Catalytic synthesis and applications. *Catal. Rev.—Sci. Eng.* **2000**, *42*, 481–510.

(24) Baronetti, G. T.; de Miguel, S. R.; Scelza, O. A.; Fritzler, M. A.; Castro, A. A. $Pt-Sn/Al_2O_3$ catalysts: Studies of the impregnation step. *Appl. Catal.* **1985**, *19*, 77–85.

(25) Prado-Burguete, C.; Linares-Solano, A.; Rodriguez-Reinoso, F.; Salinas-Martinez de Lecea, C. The effect of oxygen surface groups of the support on platinum dispersion in Pt/carbon catalysts. *J. Catal.* **1989**, *115*, 98–106.

(26) Prasomsri, T.; Shi, D.; Resasco, D. E. Anchoring Pd nanoclusters onto pristine and functionalized single-wall carbon nanotubes: A combined DFT and experimental study. *Chem. Phys. Lett.* **2010**, *497*, 103–107.

(27) Laurent, E.; Delmon, B. Study of the hydrodeoxygenation of carbonyl, carboxylic and guaiacyl groups over sulfide $CoMo/\gamma\text{-}Al_2O_3$ and $NiMo/\gamma\text{-}Al_2O_3$ catalysts. I. Catalytic reaction schemes. *Appl. Catal., A* **1994**, *109*, 77–96.

(28) Pinheiro, A.; Hudebine, D.; Dupassieux, N.; Geantet, C. Impact of oxygenated compounds from lignocellulosic biomass pyrolysis on gas oil hydrotreatment. *Energy Fuels* **2009**, *23*, 1007–1014.

(29) Philippe, M.; Richard, F.; Hudebine, D.; Brunet, S. Inhibiting effect of oxygenated model compounds on the HDS of dibenzothiophenes over $CoMoP/Al_2O_3$ catalyst. *Appl. Catal., A* **2010**, *383*, 14–23.

(30) Zhao, H. Y.; Li, D.; Bui, P.; Oyama, S. T. Hydrodeoxygenation of guaiacol as model compound for pyrolysis on transition metal phosphide hydroprocessing catalysts. *Appl. Catal., A* **2010**, *391*, 305–310.

(31) Filley, J.; Roth, C. Vanadium catalyzed guaiacol deoxygenation. *J. Mol. Catal. A: Chem.* **1999**, *139*, 245–252.

(32) Bui, V. N.; Laurenti, D.; Afanasiev, P.; Geantet, C. Hydrodeoxygenation of guaiacol with CoMo catalysts. Part I: Promoting effect of cobalt on HDO selectivity and activity. *Appl. Catal., B* **2010**, *101*, 239–245.

(33) Stagg, S. M.; Romeo, E.; Padro, C.; Resasco, D. E. Effect of promotion with Sn on supported Pt catalysts for CO_2 reforming of CH_4. *J. Catal.* **1998**, *178*, 137–145.

(34) Chiappero, M.; Do, P. T. M.; Crossley, S.; Lobban, L. L.; Resasco, D. E. Direct conversion of triglycerides to olefins and paraffins over noble metal supported catalysts. *Fuel* **2011**, *90*, 1155–1165.

(35) Zhu, X.; Mallinson, R. G.; Resasco, D. E. Role of transalkylation reactions in the conversion of anisole over HZSM-5. *Appl. Catal., A* **2010**, *379*, 172–181.

(36) Zhu, X.; Lobban, L. L.; Mallinson, R. G.; Resasco, D. E. Bifunctional hydrodeoxygenation of anisole over a $Pt/H\beta$ catalyst. *J. Catal.* **2011**, *281*, 21–29.

(37) Ferrari, M.; Maggi, R.; Delmon, B.; Grange, P. Influences of the hydrogen sulfide partial pressure and of a nitrogen compound on the hydrodeoxygenation activity of a CoMo/carbon catalyst. *J. Catal.* **2001**, *198*, 47–55.

(38) Zhao, C.; He, J.; Lemonidou, A. A.; Li, X.; Lercher, J. A. Aqueous-phase hydrodeoxygenation of bio-derived phenols to cycloalkanes. *J. Catal.* **2011**, *280*, 8–16.